A Numerically Efficient Technique for the Analysis of Metamaterial- and Metasurface-based Antennas

Abdelkhalek Nasri [1], Raj Mittra [1,2], Asim Ghalib [2], Bandar Hakim [1], and Hatem Rmili [1]

[1] Electrical and Computer Engineering Department, Faculty of Engineering
King Abdulaziz University, P.O. Box 80204, Jeddah 21589, Saudi Arabia

[2] Electrical and Computer Engineering, University of Central Florida, Orlando, FL 32816, USA
hmrmili@kau.edu.sa

Abstract ─ Metasurface-based antennas have received considerable recent attention in recent years because they are not only useful for designing new antennas, but for improving the performance of legacy designs as well. However, systematically designing these antennas is challenging because the antennas are usually multiscale in nature and they typically require a long time when simulated by using commercial solvers. In this work, we present a new approach for analyzing antennas that utilize Metasurfaces (MTSs) and Metamaterial (MTMs). The proposed method departs from the widely used technique based on an anisotropic impedance representation of the surface and relies on an equivalent medium approach instead. The principal advantage of the proposed approach is that such an equivalent medium representation can be conveniently inserted directly in commercial EM solvers, circumventing the need to develop special numerical EM simulation codes to handle metasurfaces. Several illustrative examples are presented in the paper to demonstrate the efficacy of the present approach when simulating MTS- and MTM-based antennas.

Index Terms ─ Equivalent medium, metamaterials, metasurfaces, multiscale problems, numerical simulation.

I. INTRODUCTION

Antennas based on Metasurface (MTS) and Metamaterial (MTM) antennas have received considerable recent attention in recent years, since they are not only useful for designing new antennas, but for improving the performance of legacy designs as well. This is often true for antennas designed for satellite communications, as well as 5G applications, where innovative designs are called for to replace the legacy designs.

Some recent works based on MTS-based design include Minatti [1], in which an MTS antenna was described for the enhancement of bandwidth and gain. Figure 1 shows some novel MTS antenna designs proposed by Maci in [2] for a variety of applications. A different strategy for designing high-gain antennas has been presented in [3]. It utilizes a lens-like superstrate to achieve a large gain-bandwidth product.

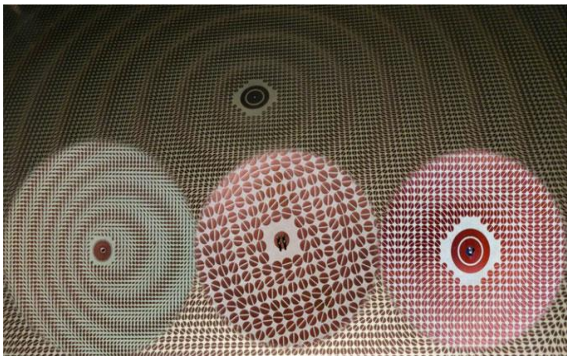

Fig. 1. Examples of metasurface-based antennas [2].

Lens antennas including flat lenses [4], Luneburg lenses [5], and others mentioned in [3], are typically fabricated by using artificially synthesized dielectrics that are also multiscale in nature; hence, in common with the MTS- and MTM-based antennas, they too are computer-intensive to simulate. Recently, some interesting methods for analyzing these metasurfaces have been reported in the literature to reduce the computational cost. Caminita in [6] have proposed a fast method for analyzing MTS antennas using the Method of Moments. In [7], Xiao has described a method utilizing surface impedance and equivalent circuit models for modulated metasurface antennas. Additionally, a literature search reveals a number of other papers which deal with the topic of MTS modeling. These include: Method of Moments using orthogonal entire domain basis Functions in [8], generalized sheet transition conditions (GSTCs) in [9], integral equation formulations based on impedance boundary condition in [10], Fourier-Bessel basis functions

Submitted On: October 16, 2020
Accepted On: March 1, 2021

https://doi.org/10.47037/2020.ACES.J.360401

in [11], dyadic Green's functions in[12] and Gaussian Ring basis functions in [13]. Additionally, the authors in [14] have used a combination method to characterize the metasurface, which utilizes the generalized sheet transition conditions (GSTCs), combined with the bi-anisotropic surface susceptibility functions.

In this work, we present a novel approach, which is altogether different in concept than the methods mentioned above. Our goal is to develop a general-purpose numerical modeling approach, for different types of multiscale antennas containing MTS and MTMs, which achieves numerical efficiency without sacrificing the accuracy. The new method we propose is referred to herein as the Equivalent Medium (ED) approach, which can be conveniently integrated with existing commercial software modules, rather than having the user to develop a new code for handling the simulation problems at hand---an important feature which is not readily available in other approaches, mentioned above. Furthermore, the proposed paradigm is useful for both electric and magnetic type elements, e.g., dipoles or loops, with little or no modification, as long as the operating frequencies are below the resonance range, which is indeed the case for most practical MTS applications, to circumvent the problem with lossy and highly dispersive nature of the MTM and MTS when operating near or above resonance. We should point out however, that the method itself works even after we go past the resonance range, though we strongly recommend that the metasurface-based antennas be used below the resonance range to avoid issues with dispersion and losses.

In general, the equivalent medium is comprised of both ε and μ that are both tensors, and they can be extracted by using inversion algorithms available in the literature [15]-[17]. However, in this work we choose an ε-only representation, which simplifies the numerical computation significantly, without compromising the accuracy of the results, as we will demonstrate below. The epsilon-only representation is referred to herein as the Equivalent Dielectric approach, which is detailed below in the next section.

The paper is organized as follows. Section II, describes the proposed approach which is applicable to a wide variety of metasurfaces; Section III demonstrates the accuracy and efficacy of the proposed method, which has previously been described in [18],[19], by presenting several examples and a comparison in terms of performance, simulation time and required memory for these examples. Finally, some conclusions are presented in Section IV.

II. PRINCIPLE OF THE EQUIVALENT DIELECTRIC APPROACH

In this section we present the basic principles of the Equivalent dielectric (ED) approach for modeling antennas with metasurfaces or metamaterials that are inherently multiscale in nature. Our core strategy for handling the problem of simulating structures containing metasurfaces or metamaterials is to replace them with an "equivalent dielectric" material slab, to be inserted later into a legacy EM simulation program, together with the antenna structure we are modeling. This strategy enables us to circumvent the need to use a fine mesh to model the multiscale geometry, which in turn requires a large number of unknowns and, hence, is both memory- and time-consuming. The principle of our proposed approach is summarized in the following.

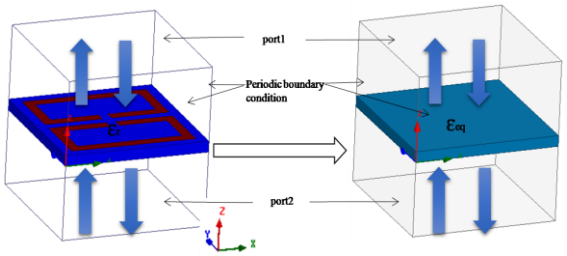

(a) (b)

Fig. 2. (a) Original unit cell of MTS with periodic boundary conditions; (b) equivalent dielectric slab.

Our first step is to determine the equivalent epsilon parameters for the original metamaterial slab. We do this by placing the unit cell of the metamaterial slab in a commercial EM simulation program and imposing the periodic boundary conditions, as shown in Fig. 2 (a). Next, we match the phase of S_{12} of the equivalent dielectric slab (see Fig. 2 (b)) is the same as with that of the original MTS medium shown in Fig. 2 (a). The thickness of the equivalent slab is typically chosen to be the same as that of the original MTM or MTS. It is worthwhile to point out that we only use an equivalent dielectric and not a combination of equivalent ε and μ, as is the usual practice. We will demonstrate below, by using several examples, that we are able to get accurate results using this approach which assumes that μ is equal to μ_0 or an appropriate constant value that we may choose. Note also that the equivalent epsilon that we derive by using the procedure described above is a function of frequency and, hence, the medium is dispersive, as the physics of the problem dictates that it would be. However, this does not create any problem when we simulate the antenna plus metasurface combination using a commercial solver, which can handle a dispersive medium in a routine manner.

In principle, for the general case, we need a 3*3 matrix to characterize the epsilon tensor of the ED in Fig. 2 (b), and it can be described by:

$$\varepsilon = \begin{pmatrix} \varepsilon_{xx} & \varepsilon_{xy} & \varepsilon_{xz} \\ \varepsilon_{yx} & \varepsilon_{yy} & \varepsilon_{yz} \\ \varepsilon_{zx} & \varepsilon_{zy} & \varepsilon_{zz} \end{pmatrix}, \quad (1)$$

where x,y and z are the three directions shown in Fig. 2.

However, in our experience it is sufficient to use either a scalar epsilon or a uniaxial one for most of the MTSs we deal with in practice. Much of the discussion presented below is limited only to those cases and it excludes the case of full tensor representation of the equivalent dielectric. The exception is the case of a chiral medium which is briefly described below by using one example in Section III.

For an isotropic material, the ε-tensor is the same in all directions, *i.e.*, $\varepsilon = \varepsilon_{xx} = \varepsilon_{yy} = \varepsilon_{zz}$. For the uniaxial case, the material is characterized by a diagonal matrix, whose diagonal elements are no longer the same:

$$\varepsilon = \begin{pmatrix} \varepsilon_{xx} & 0 & 0 \\ 0 & \varepsilon_{yy} & 0 \\ 0 & 0 & \varepsilon_{zz} \end{pmatrix}. \quad (2)$$

Finally, for MTSs that provide TE/TM and TM/TE mode conversion, we need to add off-diagonal terms in the ε-tensor to characterize them.

Figure 3 shows a metasurface comprising of square patches printed on a dielectric substrate. The geometry is x-y symmetric, and its equivalent epsilon is identical in both x- and y-directions. The extracted ε_{xx} and ε_{yy} -- they are identical for this geometry -- of the ED, derived by matching the phase of S_{12} of the unit cell of the MTS, is shown in Fig. 4 below. The phase match itself is shown in Fig. 5, which also serves to validate the equivalent dielectric concept for this example.

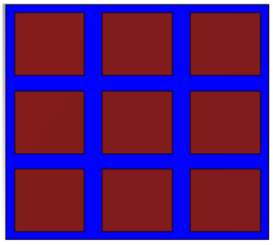

Fig. 3. Metasurface consisting of square-shaped patches.

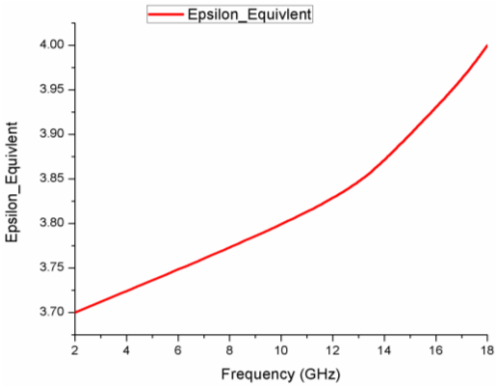

Fig. 4. Equivalent epsilon as a function of frequency for the MTS in Fig. 3.

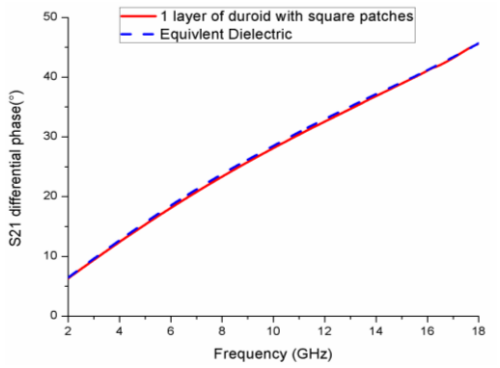

Fig. 5. Phase of S_{12} of the MTS in Fig. 3 and that of the equivalent dielectric.

A. Uniaxial metasurface

Figure 6 shows the example of a uniaxial metasurface, whose unit cell consists of two split ring patches printed on a dielectric substrate. Figure 6 highlights the extracted permittivity; ε_{xx} for the TM mode and ε_{yy} for the TE mode. For this example, it is evident from Fig. 7 that there are frequency ranges in which the permittivities are negative.

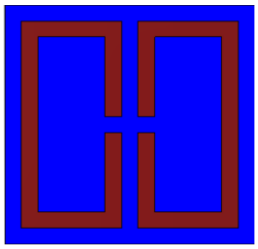

Fig. 6. Metasurface consisting of double split-rings.

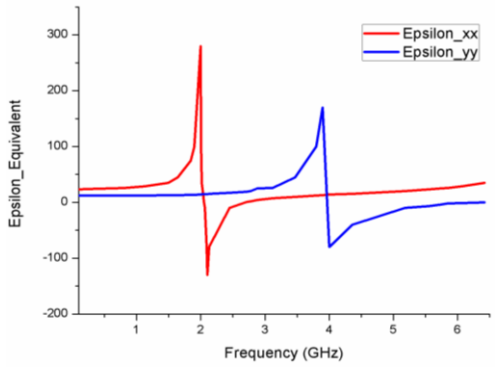

Fig. 7. Permittivities as functions of frequency for a double split-ring type of artificial medium.

Figures 8 and 9 show that both the magnitude and phase behaviors of the S-parameters of the equivalent dielectric and the original metamaterial surface agree well with each other, for both the TM and TE mode incidences. Furthermore, it is evident that the frequency

range exceeds well above the resonances of the split rings. Nonetheless, the agreement between the frequency response of the original metasurface and the equivalent dielectric representation of the same is maintained over the entire frequency range investigated, which goes well above the resonant frequencies for both ε_{xx} and ε_{yy}. This, in turn, indicates that the proposed approach is not limited to frequencies below resonance, at least for this type of MTS.

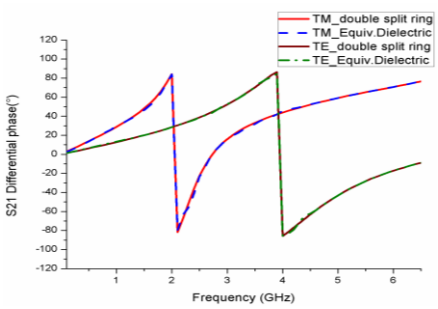

Fig. 8. Differential phase variations of the double split-ring and the Equivalent dielectric---TM and TE modes.

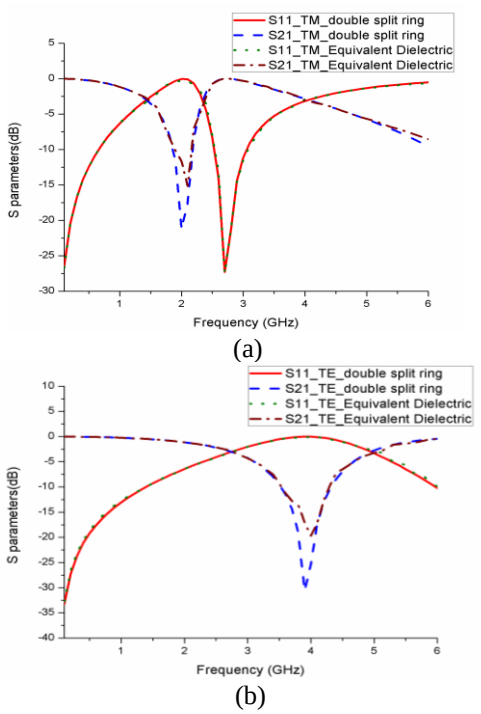

Fig. 9. Simulated S-parameter of the double split-ring and its equivalent dielectric representation: (a) TM mode and (b) TE mode.

B. Equivalent dielctric representation of Chiral metasurfaces

For the final example presented in this work, we consider a chiral type of dielectric MTS, which has been discussed in [19]. The authors in [19] have proposed a new design of an all- dielectric chiral metasurface based on elliptic dielectric resonators, which realizes circular dichroism proprieties over the frequency band of 10-20GHz.

For this type of MTS, neither the scalar nor the uniaxial representation of the epsilon tensor is adequate, and we must include off-diagonal terms in the epsilon tensor to accurately represent the TE/TM and TM/TE conversion properties of the surface. Figure 10 shows the layout of the chiral unit cell of the MTS. Figures 11 (a) and (b) present the extracted equivalent permittivity of the tensor representation. The ε_{xx} and ε_{yy} extracted parameters characterize the TM and TE modes, respectively, while the ε_{xy} and ε_{yx} parameters are associated with the TM/TE and TE/TM mode conversions, respectively.

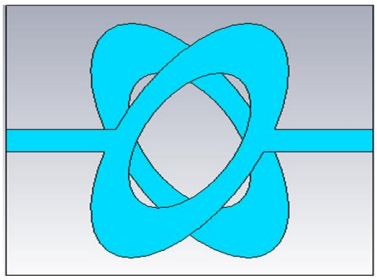

Fig. 10. Dielectric Chiral metasurface [19].

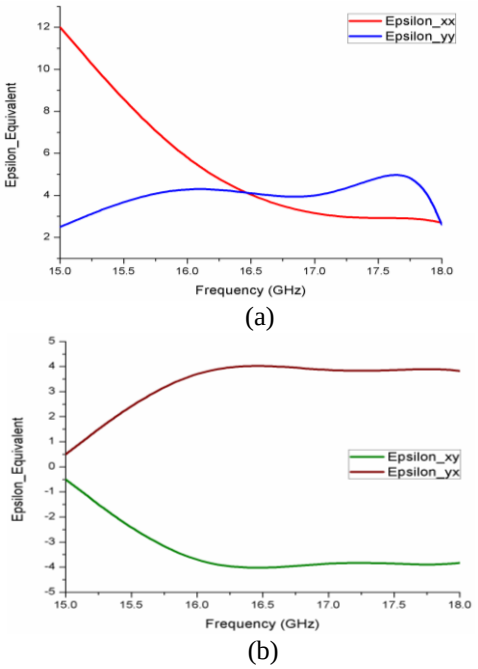

Fig. 11. Permittivities as functions of frequency for the dielectric Chiral medium shown in Fig. 10: (a) ε_{xx} and ε_{yy}; (b) ε_{xy} and ε_{yx}.

Figure 12 shows that the results for the differential phases of the TM and TE modes exhibit good agreement between the original and equivalent dielectric media. In addition, Fig. 13 demonstrates that the magnitude plots also agree with each other quite well over the entire frequency range investigated.

III. APPLICATIONS: CASE EXAMPLES

In this section we present several case examples of antennas with metasurfaces and metamaterial mediums, with a view to demonstrating the efficiency and accuracy of the proposed ED technique for modeling the metasurface type of multiscale problems.

A. Metasurfaces based antenna

For the first example, we consider a microstrip patch antenna with an MTS superstrate, as shown in Fig. 14. The unit cell of the MTS is a metallic cross printed on a dielectric substrate. Comparisons between the S-parameters and gain values of the original and equivalent configurations are shown in Figs. 15 and 16, respectively. We note that the two results are in good agreement over the entire frequency range of 1 to 5 GHz.

Table 1 compares the times needed to simulate the original design and its equivalent counterpart and shows that a 66% improvement is achieved.

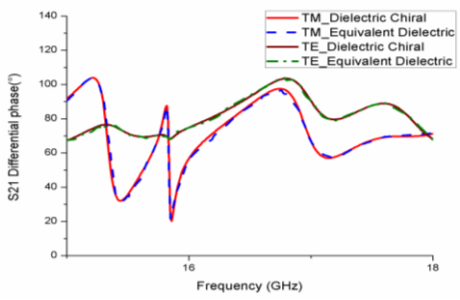

Fig. 12. Differential phase variations of S_{21} of the unit cell in Fig. 10 and that of the ED, for the TM and TE modes.

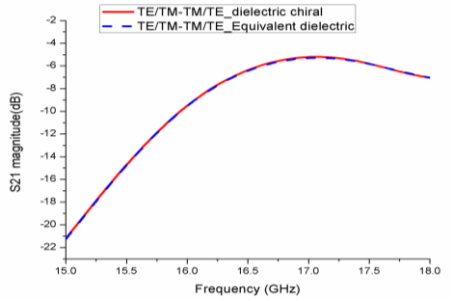

Fig. 13. Simulated magnitudes of the unit cell in Fig. 10 and the ED for TE/TM and TM/TE modes.

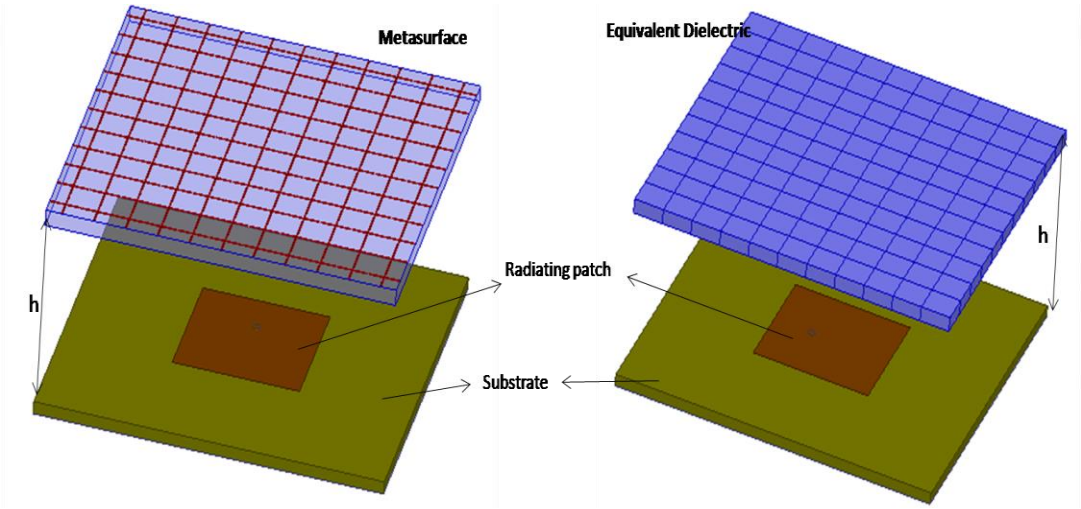

(a) (b)

Fig. 14. Patch antenna with different superstrate: (a) metasurface and (b) equivalent dielectric.

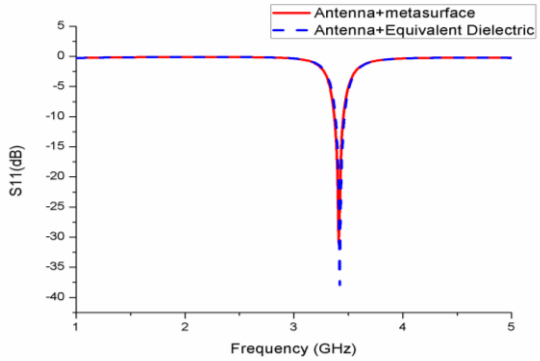

Fig.15. Simulated S parameters of the patch antenna with different superstrate.

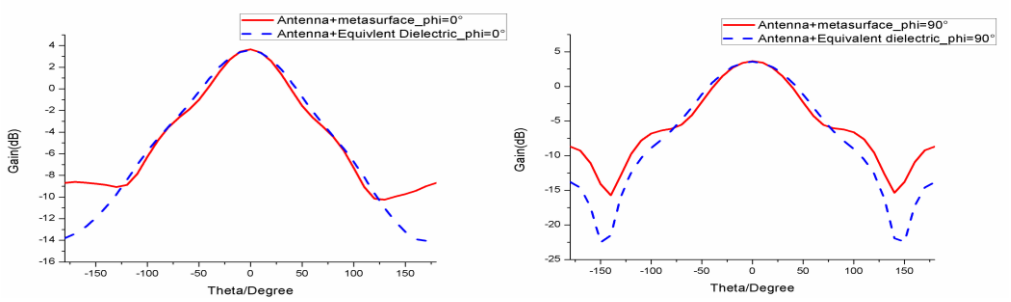

(a) (b)

Fig. 16. Simulated gain of the patch antenna with different superstrate at 3.36 GHz: (a) E plane and (b) H plane.

Table 1: Comparison of simulation times between the equivalent dielectric approach and the original design of patch antennas

	Antenna Only	**Antenna+Metasurface**	**Antenna+Equivalent Dielectric**
Frequency range (GHz)	1-5	1-5	1-5
Resonant frequency (GHz)	3.36	3.42	3.42
Gain (dB)	2.89	3.65	3.56
Simulation Time (hh:mm:ss)	00:03:37	00:25:02	00:07:47

For the second example, we consider a horn antenna with a metasurface panel placed just in front of its aperture. The original design and its equivalent dielectric counterpart are shown in Figs. 17 (a) and (b), respectively. Figures 18 and 19 plot the S-parameters and radiation patterns of the two antenna systems and demonstrate that they compare well with each other.

Next, Table 2 compares the simulation times for the two configurations, and demonstrates that the equivalent dielectric approach is faster by a factor of 23 in terms of the simulation time for a single layer of metasurface, and that this factor jumps to 162 for a double-layer metasurface.

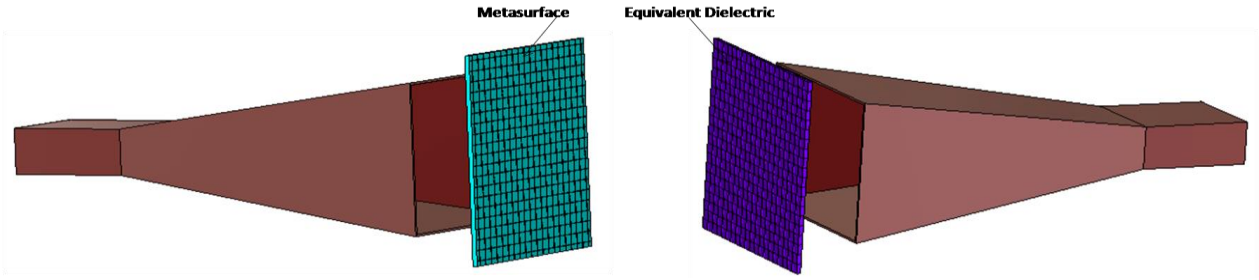

(a) (b)

Fig. 17. Horn antenna with different superstrates: (a) metasurface and (b) equivalent dielectric.

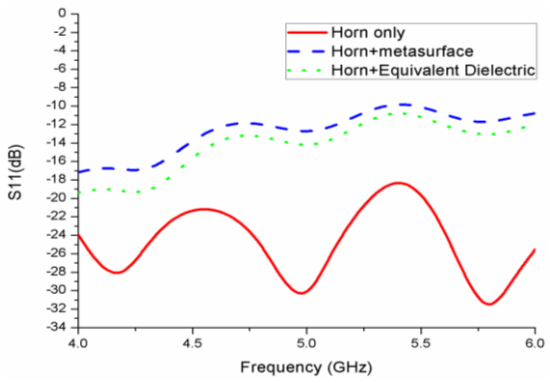

Fig. 18. Simulated S parameters of the horn antennas with different superstrate.

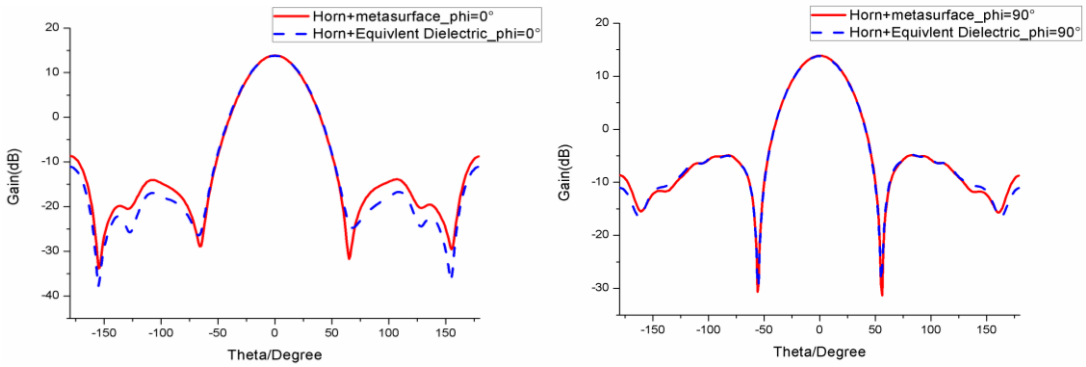

(a) (b)

Fig. 19. Simulated gain of the horn antennas with different superstrates at 5 GHz: (a) E-plane and (b) H-plane.

Table 2: Comparison of simulation times between the equivalent dielectric approach and the original design of horn antennas

	Antenna Only	**Horn+Metasurface**	**Horn+Equivalent Eielectric**	**Horn+2 Layers of Metasurface**	**Horn+2 Layers of Equivalent Dielectric**
Frequency range (GHz)	4-6	4-6	4-6	4-6	4-6
Gain (dB)	13.1	13.9	13.8	14.04	14.1
Simulation Time (hh:mm:ss)	00:03:30	02:20:00	00:06:00	16:17:00	00:12:00

Next, we turn to a geometry which is even more complex than the ones we have considered thus far. Figure 20 shows a 3x3 microstrip patch antenna array (MPA) covered by a metasurface superstrate comprising of 8*12 unit cell elements. Once again, we replace the superstrate with an equivalent dielectric slab, simulate the two configurations and compare the accuracies as well as relative numerical efficacies of the two approaches. Figures 21 and 22 show good agreement in both the results for the reflection coefficient as well as the radiations patterns, in both E-and H-planes, of the two antenna configurations depicted in Fig. 20. Table 3 compares the CPU time and RAM requirements of the original metasurface-based antenna array and its Equivalent Dielectric counterpart. We observe that the simulation time using the proposed approach decreases almost by a factor of 5, down to 15 hours from 73, and the max RAM required is also reduced to 24.4 GB from the original 91.3 GB.

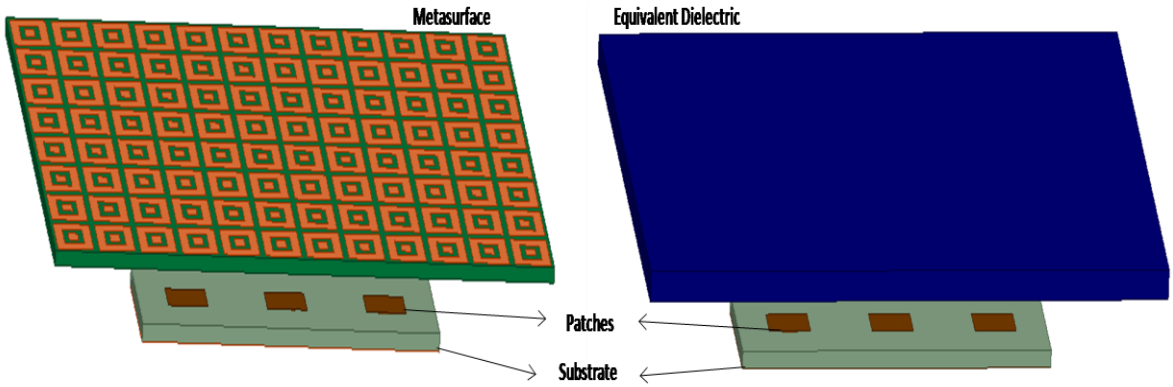

(a) (b)

Fig. 20. Three-element MPA with different superstrates: (a) metasurface and (b) equivalent dielectric (ED).

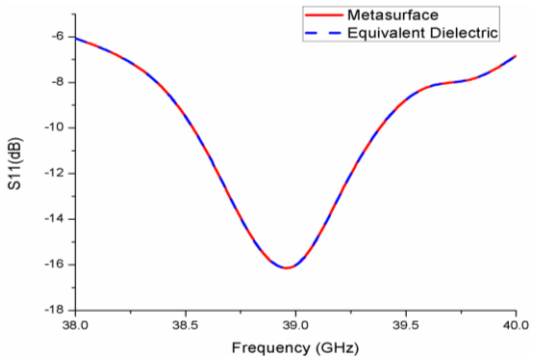

Fig. 21. Simulated S parameters of the three-element patch array with different superstrates.

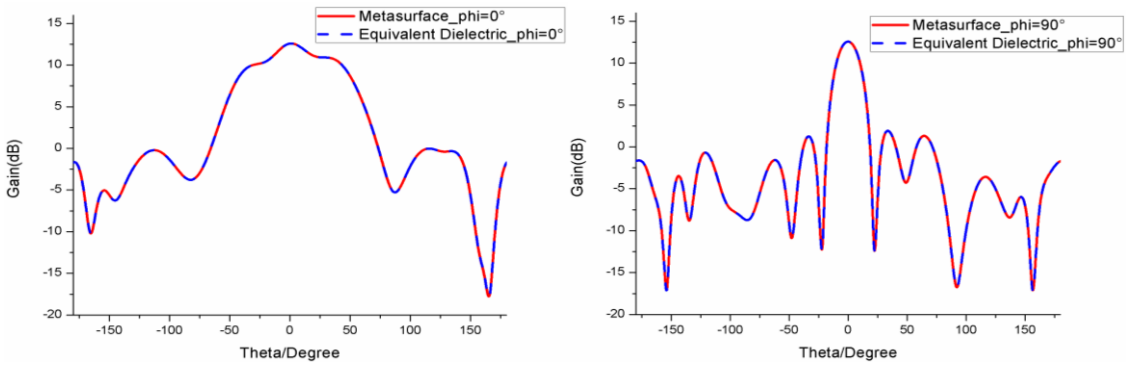

(a) (b)

Fig. 22. Simulated gain of the three-element patch with MTS and ED superstrates at 39 GHz: (a) E-plane and (b) H-plane.

Table 3: Comparison of CPU times and required RAM between the equivalent dielectric approach and the original design of metasurface superstrates antenna array

	Max RAM (GB)	**Real Time**	**CPU Time**
Three-element patch	1.04	0:14:04	0:13:59
Three element patch+Metasurface	91.3	72:55:04	95:51:09
Three element patch+Equivalent Dielectric	24.4	14:56:47	16:57:22

B. Flat lens application

For the final example, we consider a metamaterial-based flat lens, designed to replace the conventional convex dielectric lens to reduce the fabrication cost. The building block of the lens is shown in Fig. 24, which is a hollowed-out dielectric cuboid, and its Equivalent Dielectric model is shown in Fig. 23. So, our study displays that while the performances in terms of S_{11} of the horn and its gain enhancement with lens, shown in Figs. 25 and 26, respectively, are in good agreement over a broad frequency range of 12-18 GHz. However, the simulation time and memory requirement for the equivalent dielectric model are less by factors of 13x and 7x, respectively, than that for the original lens with air holes.

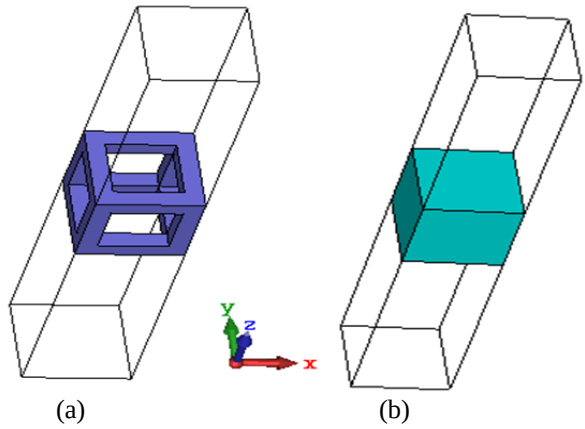

Fig. 23. Unit cell design: (a) dielectric with air hole, and (b) equivalent dielectric.

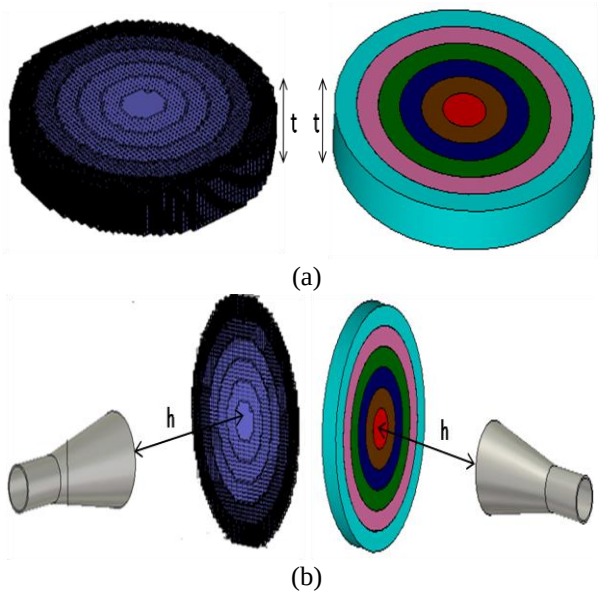

Fig. 24. Lenses with horn feed: (a) isometric view of flat lenses, and (b) lenses in front of the feed horn.

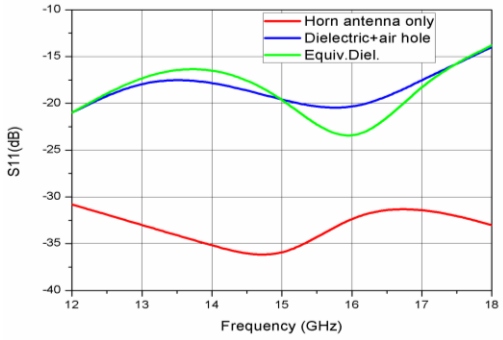

Fig. 25. S-parameters for horn and horn+lens combinations.

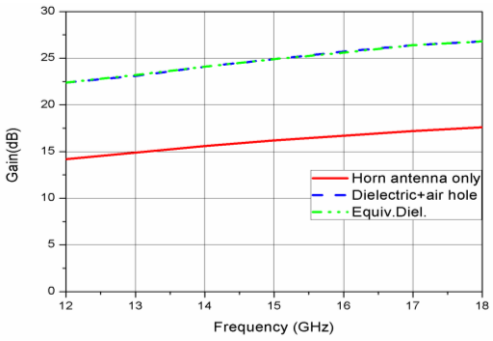

Fig. 26. Gain comparison of horn alone and horn+lenses.

IV. CONCLUSION

A novel approach for numerically efficient simulation of metamaterial- and metasurface-based antennas has been presented in this work. It relies on the use of an equivalent dielectric representation to characterize antennas with metasurfaces and metamaterials that are often multiscale in nature and, hence, are time-consuming and memory-intensive to simulate. Not only does the proposed approach offer a significant advantage over conventional brute-force type of techniques for multi-scale problems, it also assures that the accuracy of the results is not sacrificed in the process. The efficiency of the proposed ED method was tested for several different problems and it was found to yield accurate results while reducing the computational resources significantly. The reduction was 66% and 83%, respectively, for the single patch antenna and the 3x1 array, both with an MTS superstrate included for performance enhancement. For the horn antenna with single- and double-layer MTS covers, the computational resource requirement was reduced by factors of 23 and 162, respectively. Yet another significant advantage of the proposed technique is that the equivalent dielectric model can be directly inserted in commercial solvers; hence, no new special-purpose EM simulation code needs to be developed to handle multiscale problems when using the proposed approach.

ACKNOWLEDGEMENT

This project was funded in part by the Deanship of Scientific Research (DSR), King Abdulaziz University, Jeddah, Saudi Arabia, under Grant No. **RG-2-135-38**. The authors are pleased to acknowledge the technical and financial support from the DSR.

REFERENCES

[1] G. Minatti, M. Faenzi, M. Sabbadini, and S. Maci, "Bandwidth of gain in metasurface antennas," *IEEE Transactions on Antennas and Propagation*, vol. 65, no. 6, pp. 2836-2842, June 2017.

[2] M. Faenzi, G. Minatti, D. G.-Ovejero, F. Caminita, E. Martini, C. D. Giovampaola, and S. Maci, "Metasurface antennas: New models, applications and realizations," *A Nature Research Journal*, vol. 9, pp. 1-14, July 2019.

[3] A. A. Baba, R. M. Hashmi, and K. P. Esselle, "Achieving a large gain-bandwidth product from a compact antenna," *IEEE Transactions on Antennas and Propagation*, vol. 65, no. 7, pp. 3437-3446, July 2017.

[4] M. Imbert, J. Romeu, M. B.-Escudero, M.-T. Martinez-Ingles, J.-M. M. Garcia-Pardo, and L. Jofre, "Assessment of LTCC-based dielectric flat lens antennas and switched-beam arrays for future 5G millimeter-wave communication systems," *IEEE Transactions on Antennas And Propagation*, vol. 65, no. 12, pp. 6453-6473, Dec. 2017.

[5] A. Sayanskiy, S. Glybovski, V. Akimov, D. Filonov, P. Belov, and I. Meshkovskiy, "Broadband 3D Luneburg lenses based on metamaterials of radially diverging dielectric rods," *IEEE Antennas and Wireless Propagation Letters*, vol. 16, pp. 1520-1523, Jan. 2017.

[6] F. Caminita, E. Martini, G. Minatti, and S. Maci, "Fast integral equation method for metasurface antennas," *2016 URSI International Symposium on Electromagnetic Theory (EMTS)*, Sep. 2016.

[7] X. Liu, F. Yang, S. Xu, and M. Li, "Design method for modulated metasurface antennas composed of anisotropic elements based on generalized boundary conditions," *Antennas and Wireless Propagation Letters*, vol. 18, no. 9, pp. 1848-1852, July 2019.

[8] M. Bodehou, D. González-Ovejero, C. Craeye, and I. Huynen, "Method of moments simulation of modulated metasurface antennas with a set of orthogonal entire-domain basis functions," *IEEE Transactions on Antennas and Propagation*, vol. 1, no. 1, pp. 1-12, Jan. 2018.

[9] S. Sandeep and S. Y. Huang, "Simulation of circular cylindrical metasurfaces using GSTC-MoM," *IEEE Journal on Multiscale and Multi-physics Computational Techniques*, vol 3, pp. 185-192, Nov. 2018.

[10] M. A. Francavilla, E. Martini, S. Maci, and G. Vecchi, "On the numerical simulation of metasurfaces with impedance boundary condition integral equations," *IEEE Transactions on Antennas and Propagation*, vol. 63, no. 5, pp. 2153-2161, May 2015.

[11] M. Bodehou, C. Craeye, H.-B. Van, and I. Huynen, "Fourier-Bessel basis functions for the analysis of elliptical domain metasurface antennas," *IEEE Antennas and Wireless Propagation Letters*, vol. 1, pp. 1-4, 2018.

[12] F. Liang, G. W. Hanson, A. B. Yakovlev, G. Lovat, P. Burghignoli, R. Araneo, and S. A. H. Gangaraj, "Dyadic Green's functions for dipole excitation of homogenized metasurfaces," *IEEE Transactions on Antennas And Propagation*, vol. 64, no. 1, pp. 167-178, Jan. 2016.

[13] D. G.-Ovejero and S. Maci, "Gaussian ring basis functions for the analysis of modulated meta-surface antennas," *IEEE Transactions on Antennas and Propagation*, vol. 63, no. 9, pp. 3982-3993, 2018.

[14] Y. Vahabzadeh , N. Chamanara, K. Achouri, and C. Caloz, "Computational analysis of meta-surfaces," *IEEE Journal on Multiscale and Multiphysics Computational Techniques*, vol 3, pp. 37-49, Apr. 2018.

[15] D. R. Smith, S. Schultz, P. Markos, and C. M. Soukoulis, "Determination of effective permittivity and permeability of metamaterials from reflection and transmission coefficients," *Physical Review B*, vol. 65, Apr. 2002.

[16] X. Chen, T. M. Grzegorczyk, B.-I. Wu, J. Pacheco, Jr., and J. A. Kong, "Robust method to retrieve the constitutive effective parameters of metamaterials," *Physical Review E*, vol. 70, 016608, 2004.

[17] D. R. Smith, D. C. Vier, T. Koschny, and C. M. Soukoulis, "Electromagnetic parameter retrieval from inhomogeneous metamaterials," *Physical Review E*, vol. 71, 036617, 2005.

[18] A. Nasri, R. Mittra, H. Rmili, "Categorizing metamaterials by using equivalent dielectric approach," *2019 IEEE International Symposium on Antennas and Propagation and USNC-URSI Radio Science Meeting*, Oct. 31, 2019.

[19] A. Nasri and R. Mittra, "A numerically efficient technique for the analysis of metamaterial- and metasurface-based antennas," *2020 14th European Conference on Antennas and Propagation (EuCAP)*, July 8, 2020.

[20] A. Yahyaoui and H. Rmili, "Chiral all-dielectric metasurface based on elliptic resonators with circular dichroism behavior," *International Journal of Antennas and Propagation*, vol. 2018, pp. 1-7, 2018.